Chemical Engineering Journal 431 (2022) 133460

Contents lists available at ScienceDirect

Chemical Engineering Journal

journal homepage: www.elsevier.com/locate/cej

A strong underwater adhesive that totally cured in water

Yonggan Yan [a], Jun Huang [a,b,*], Xiaoyong Qiu [c], Dexuan Zhuang [d], Hanlian Liu [a], Chuanzhen Huang [e], Xunwei Wu [d], Xin Cui [f]

[a] Key Laboratory of High Efficiency and Clean Mechanical Manufacture of Ministry of Education, School of Mechanical Engineering, Shandong University, Jinan, Shandong 250061, China
[b] Key Laboratory of Icing and Anti/De-icing, China Aerodynamics Research and Development Center, Mianyang, Sichuan 621000, China
[c] Key Laboratory of Colloid and Interface Chemistry of Ministry of Education, School of Chemistry and Chemical Engineering, Shandong University, Jinan, Shandong 250100, China
[d] Department of Tissue Engineering and Regeneration, School and Hospital of Stomatology, Cheeloo College of Medicine, Shandong University & Shandong Key Laboratory of Oral Tissue Regeneration and Shandong Engineering Laboratory for Dental Materials and Oral Tissue Regeneration, Jinan, China
[e] School of Mechanical Engineering, Yanshan University, Qinhuangdao 066004, China
[f] Advanced Interdisciplinary Technology Research Center, National Innovation Institute of Defense Technology, Beijing 100071, China

ARTICLE INFO

Keywords:
Underwater adhesion
Isocyanate groups
Adhesion mechanism
Chemical crosslinks
Hydrogen bonds

ABSTRACT

Underwater adhesives have drawn enormous interests for biomedical and engineering applications. In this work, a strong underwater adhesive is developed by addition reaction between bis(3-aminopropyl) terminated polydimethylsiloxane (PDMS) and hexamethylene diisocyanate (HDI). The PDMS-based adhesive was totally cured in aqueous solutions and exhibited strong adhesion with various substrates. The highest underwater adhesion strength of the adhesive on polyethylene terephthalate (PET) substrate reached 2.8 MPa, which is comparable with those commercial glues that cured in air. Such strong underwater adhesion is mainly caused by the combination of chemical crosslinks, hydrogen bonds and other physical interactions. Further study reveals that increasing the curing temperature can decrease the mechanical strength of the adhesive, which leads to a decrease in adhesion strength. Moreover, increasing the salt concentration in aqueous solution would screen the electrostatic charges at the interface and impair the underwater adhesion. Besides, the tensile adhesion tests suggested that the underwater adhesion strength was enhanced by 3 times as the curing time extended from 3 h to 6 h. The increased adhesion is mainly caused by the enhanced mechanical strength of the polymeric adhesive as well as the increased interactions at the adhesive-substrate interface. In addition, the strong adhesion force of the adhesive is also demonstrated from the microscale by employing atomic-force-microscope force measurement. This work provides both practical and fundamental insights into developing underwater adhesives with strong adhesion.

1. Introduction

Underwater adhesion plays an essential role in biomedical and engineering fields including biological tissues, biomedical devices in human body, and underwater soft robotics [1–3]. However, it is a great challenge to develop universal adhesives with strong underwater adhesion due to the thin hydration layer covering substrate surface under aqueous solutions [4,5]. To date, great efforts have been dedicated to understanding the underwater adhesion mechanism. Inspired by the marine organisms like sandcastle worms, mussels and tunicate, researchers have revealed that the underwater adhesion of the marine creatures rely on the combination of various interactions [5–8]. The interactions mainly include electrostatic interactions, metal coordination, hydrogen bonds, hydrophobic forces, π–π interactions, cation–π complexation, and dynamic covalent crosslinks [2,5,9–12]. Various underwater adhesives have been developed by employing these interactions.

Recently, an instant underwater adhesive with tunable optical and electrochromic properties has been fabricated by mixing silicotungstic acid and poly(ethylene glycol)-block-poly(propylene glycol)-block-poly (ethylene glycol) [13]. The adhesive exhibits a underwater adhesion of 479.6 kPa on the poly(methyl methacrylate) substrate due to the synergy effects of hydrogen-bonding interaction and hydrophobic interaction [13]. Inspired by mussels, dopamine has been used to develop

* Corresponding author.
E-mail address: jun.huang@email.sdu.edu.cn (J. Huang).

https://doi.org/10.1016/j.cej.2021.133460
Received 31 August 2021; Received in revised form 16 October 2021; Accepted 2 November 2021
Available online 8 November 2021

various mussel-inspired adhesives that exhibit excellent underwater adhesion [6,7,14,15]. In addition, a thermoresponsive adhesive has been fabricated by combining poly(*N*-isopropylacrylamide) with oppositely charged polyelectrolytes, which can bond to different surfaces in the presence of water [16]. In another study, a new strategy is proposed to develop underwater adhesive by copolymerization of cationic and aromatic monomers, and the fabricated adhesive exhibits an adhesion strength of 180 kPa due to interfacial electrostatic and hydrophobic interactions [17]. Besides, it is reported that by grafting a hyperbranched polymer with hydrophilic adhesive catechol branches, a water-triggered universal polymer adhesive has been developed, which can be used to seal the wound and rapidly stop visceral bleeding [18].

Despite of the recent progresses on developing functional adhesives, most of the reported adhesives only exhibit weak wet adhesion and are not able to totally cure in water. And a few recently reported adhesives that can be cured in water exhibt limited adheison strength of less than 1 MPa. For these adhesives, non-covalent interactions play dominant roles at the interface, which may not be strong enough for practical applications. The combination of covalent crosslinks, hydrogen bonds and other physical interactions is an effective way in developing strong underwater adhesives. Hexamethylene diisocyanate (HDI) contains isocyanate groups, which can form covalent crosslinks with various function groups (e.g —OH and —NH_2) on the substrate surface. However, HDI is unable to adhere substrates underwater due to its rapid reaction with water molecules. A general strategy is to incorporate an aminopropyl terminated polymer with HDI to achieve strong underwater adhesion. Bis(3-aminopropyl) terminated polydimethylsiloxane (PDMS) consisting of a hydrophobic silicon-oxygen backbone and two terminated primary amines is an excellent candidate for crosslinking with HDI. In addition, the amino groups and urea bonds can form hydrogen bonds at the interface, which also contributes to the interfacial adhesion. Therefore, the PDMS-based polymer incorporating with HDI could be a reasonable choice for fabricating underwater adhesives.

In this work, a type of PDMS-based adhesive is developed by combining covalent crosslinks with hydrogen bonds and other physical interactions. The adhesive can be totally cured in aqueous condition and exhibits strong underwater adhesion with various substrates. After curing in water, both tensile and lap-shear adhesion tests are carried out to understand the adhesion behavior of the adhesive on different substrates. The adhesion behavior with curing time has been systematically analyzed. In addition, the effect of salt concentration and temperature as well as the underwater adhesion mechanisms of the adhesive are systematically investigated. Atomic force microscopy (AFM) force measurements are employed to analyze the adhesion behavior of the adhesive from the microscale. Overall, this work aims at fabricating an underwater adhesive with strong adhesion strength on various substrates and studying the mechanism of underwater adhesion, which could provide practical and fundamental insights into designing strong underwater adhesives for biomedical and engineering applications.

2. Materials and methods

2.1. Materials

Bis(3-aminopropyl) terminated polydimethylsiloxane (PDMS, Mw ~ 3000) was purchased from Gelest, Inc. (Morrisville, USA). Hexamethylene diisocyanate (HDI, 99%) was purchased from Shanghai Macklin Biochemical Technology Co., Ltd (Shanghai, China). Tetrahydrofuran (THF, 99.5%) was purchased from Sinopharm Chemical Reagent Co., Ltd (Shanghai, China). All reagents in this work were used as received without further purification.

2.2. HDI-PDMS polymeric adhesive preparation

The HDI-PDMS polymeric adhesive was fabricated by dissolving PDMS and HDI in THF. Typically, 0.1 mmol HDI (0.0168 g) and 0.1 mmol PDMS (3 g) were added to THF (3.0168 g), followed by stirring for 2 h and degassing for 15 min. After that, the fabricated HDI-PDMS polymeric adhesive was stored at −70 °C for further tests. In addition, the HDI-PDMS adhesives with different molar ratios of HDI: PDMS = 1:2, 1:1, 2:1 and 4:1 were also fabricated.

2.3. Characterizations

Fourier transform infrared (FTIR) spectra was used to record the function groups of the adhesive on a Tensor II infrared spectrometer (Bruker Company, Germany). The KBr disks were prepared by mixing the testing samples with KBr powders, followed by drying with an infrared lamp for 5 min and pressing at 10-ton load. After that, the KBr disks were placed into the FTIR instrument for recording the infrared spectra. The X-ray photoelectron spectroscopy (XPS) was used to further examine the surface elemental composition of the adhesive on an X-ray photoelectron spectrometer (Thermo Scientific K-Alpha, USA). Thermogravimetric (TG) experiments were conducted on a thermal analysis system (STA 449 F3, NETZSCH) at a heating rate of 10 °C/min. Water contact angles were measured using a contact angle meter (SDC-200S, Dongguan Shengding Precision Instrument Co., Ltd, China).

2.4. Rheology analysis

A rheometer (MCR 302, Anton Paar) was used to monitor the change of viscosity and modulus during the reaction of PDMS with HDI. Typically, 0.15 mL PDMS and 5μL HDI were placed separately on the rheometer holder. After that, a 25 mm parallel plate was used to conduct the experiment. The viscosity was measured at a shear rate of 5 s^{-1}. The modulus was measured at a fixed strain ($\gamma = 1\%$) and frequency ($f = 1$ Hz). In addition, the modulus tests of the cured HDI-PDMS hydrogel at a temperature range of 25 °C ~ 100 °C were also conducted.

2.5. Underwater adhesion tests

The underwater adhesion tests were measured using a universal testing machine (ZLC-2D, Jinan XLC Testing Machine Co., Ltd, China) at a loading rate of 50 mm/min with a 2.5 kN load cell. The underwater adhesion properties of the adhesive on various substrates including iron, glass, polyethylene terephthalate (PET), and polytetrafluoroethylene (PTFE) were evaluated by both tensile and lap-shear adhesion tests. The detailed characterizations of those substrates including surface components, morphologies and water contact angles are shown in **Figure S1** and **Table S1** in **Supporting Information**. The adhesive samples were cured and tested underwater. Typically, 0.05 mL HDI-PDMS polymeric adhesive was injected and painted on a rod surface in a customized chamber filled with water. After that, another rod with a diameter of 15 mm was immediately pressed against the surface at a normal load of 5 N for 20 s. After curing for 24 h underwater at room temperature (25 °C), the prepared samples were used for tensile tests. Similarly, the underwater lap-shear adhesion tests were conducted with a square contact area of 12 mm × 12 mm after 24 h curing at room temperature (25 °C). In addition, the underwater adhesion strength of the adhesive on iron substrates at different curing times and temperatures was also investigated. The underwater adhesion tests in salt solutions (deionized water and NaCl) were also conducted. The adhesion tests were repeated three times under the same condition for checking the reproducibility of the adhesion.

2.6. AFM force measurements

The adhesion force between the HDI-PDMS adhesive and glass surface was probed using an AFM (CSPM5500, Beijing Nano-Instruments, Ltd., China) through a Si tip with the spring constant of 40 N/m. Typically, a HDI-PDMS precursor solution was prepared by dissolving 0.1 mmol HDI (0.0168 g) and 0.1 mmol PDMS (3 g) in 27.15 g acetone. Then

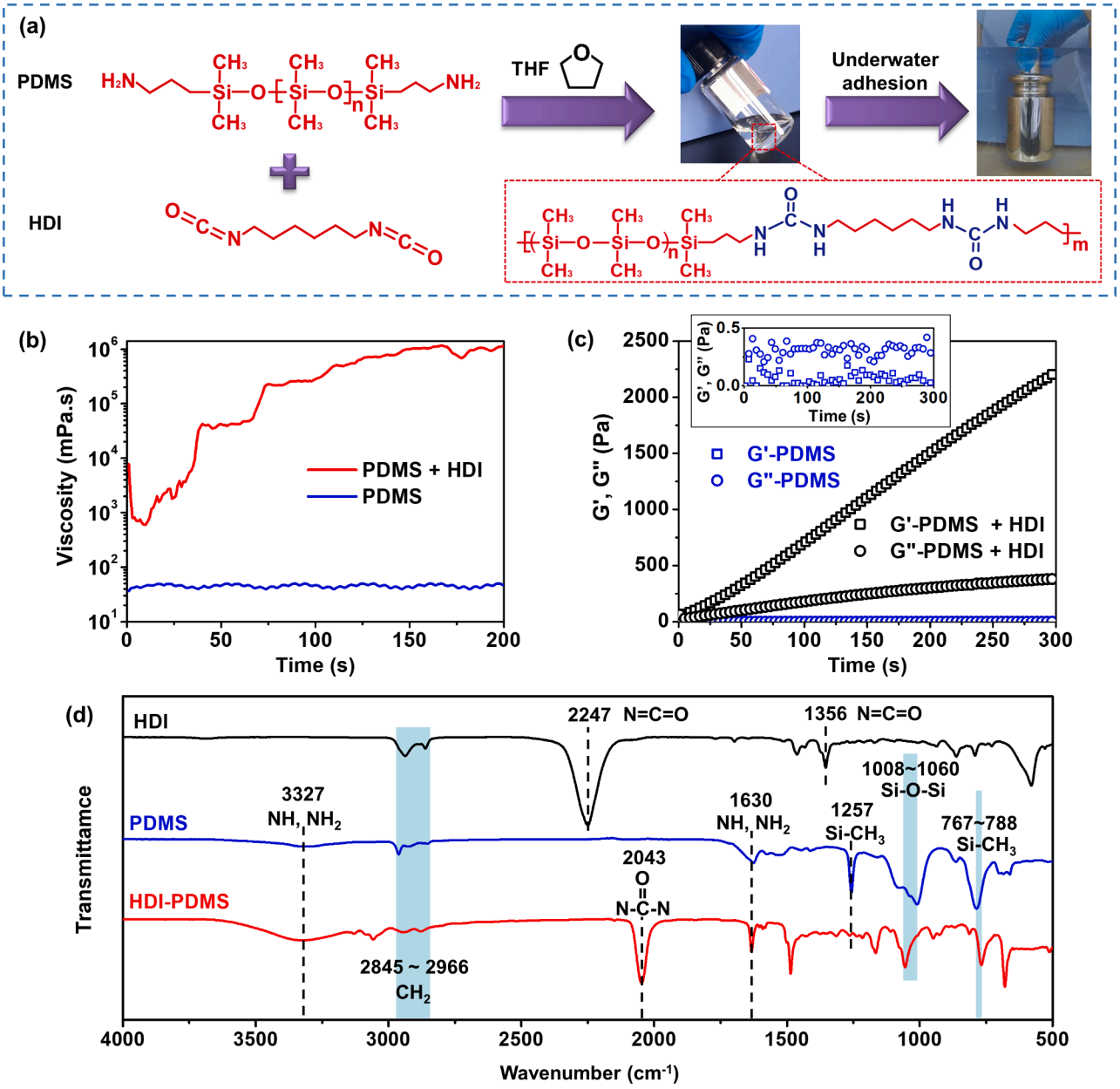

Fig. 1. (a) Schematic illustration of fabricating the polymeric adhesive. (b) The viscosity of the pure PDMS and the PDMS mixed with HDI. (c) Storage modulus (G′) and loss modulus (G″) of pure PDMS and PDMS mixed with HDI. (d) FTIR spectra of the HDI-PDMS adhesive.

the HDI-PDMS precursor solution was coated on the AFM tip, followed by evaporation of the acetone at 25 °C for 15 min (see **Figure S2**). After removing the acetone, the tip with HDI-PDMS was used to obtain the typical force-separation curves with the glass surface. In addition, the adhesion force between PDMS and glass surface was also measured.

3. Results and discussion

3.1. Preparation of the HDI-PDMS polymeric adhesive

As shown in Fig. 1**a**, the HDI-PDMS polymeric adhesive is prepared by dissolving the bis(3-aminopropyl) terminated PDMS and HDI in THF. The HDI-PDMS polymeric chains are formed through the reaction between the isocyanate group (—N═C═O) in HDI and the amino groups ($—NH_2$) in the PDMS. The fabricated HDI-PDMS polymer exhibits excellent underwater adhesion, which can instantly and firmly adhere two substrates underwater. During the reaction process between PDMS and HDI, the viscosity and modulus of the polymer would increase dramatically, which can be detected using a rheometer. As shown in Fig. 1**b**, the viscosity of pure PDMS is 40 ~ 50 mPa·s and remains as a constant with time increasing. However, the viscosity of PDMS mixed with HDI is quite high and increased from ~ 600 mPa·s to ~ 10^6 mPa·s within 150 s. The dramatic increase in viscosity is caused by the growth of polymer chains and the formation of solid HDI-PDMS during the reaction between PDMS and HDI. Fig. 1**c** illustrates the change of storage modulus (G′) and loss modulus (G″) of the polymer during reaction. For pure PDMS, both G′ and G″ of the liquid are extremely low (0 ~ 0.5 Pa) and maintain constant with time. The G′ and G″ of the PDMS mixed with HDI are much higher than that of pure PDMS. For the case of PDMS mixed with HDI, G′ is larger than G″, indicating PDMS has reacted with HDI and solid phase was gradually formed. In addition, both G′ and G″ dramatically increased with time due to the reaction between PDMS and HDI. Fig. 1**d** shows the FTIR spectra of HDI, PDMS and the fabricated HDI-PDMS adhesive. The absorption peak at 2845 ~ 2966 cm^{-1} is

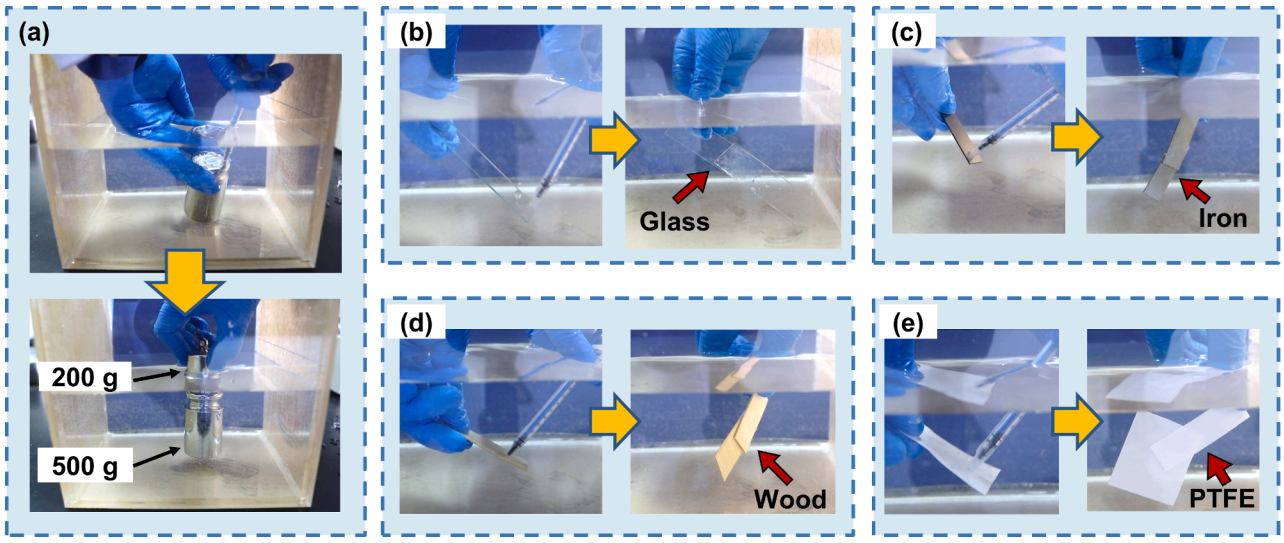

Fig. 2. Underwater adhesive properties of the polymeric HDI-PDMS adhesive. (a) The HDI-PDMS adhesive can instantly and firmly adhere two weights (200 g and 500 g, and the contact area is 415.5 mm^2), (b) glass, (c) iron, (d) wood and (e) PTFE underwater.

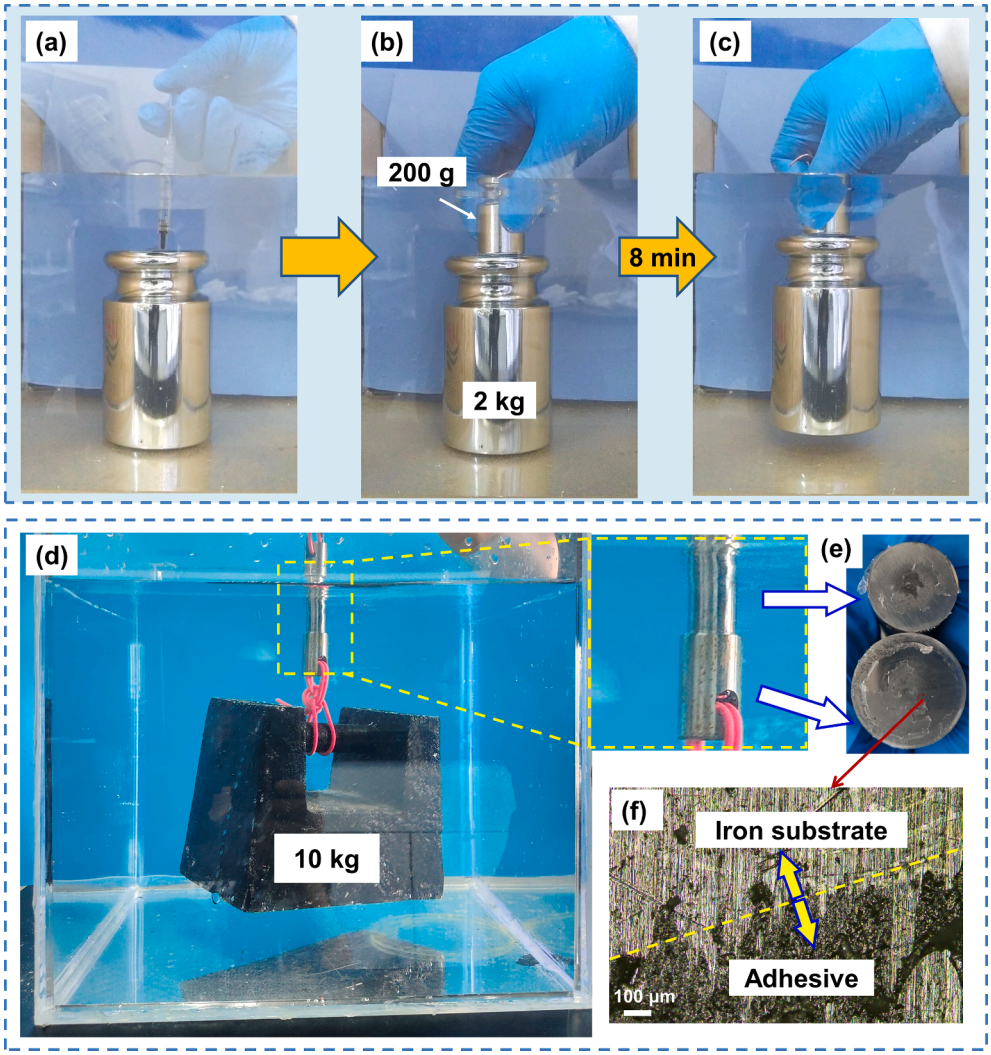

Fig. 3. (a) The HDI-PDMS polymeric adhesive was directly injected and painted on a 2 kg weight underwater, and then (b) a 200 g weight was immediately pressed against the surface. (c) The 2 kg weight can be easily lifted after curing in water for 8 min. The contact area is 415.5 mm^2. (d) A 10 kg weight can be easily lifted after curing for 24 h by two adhered iron substrates with the contact area of 176.7 mm^2. (e-f) Mixed interfacial failure was observed at the interface.

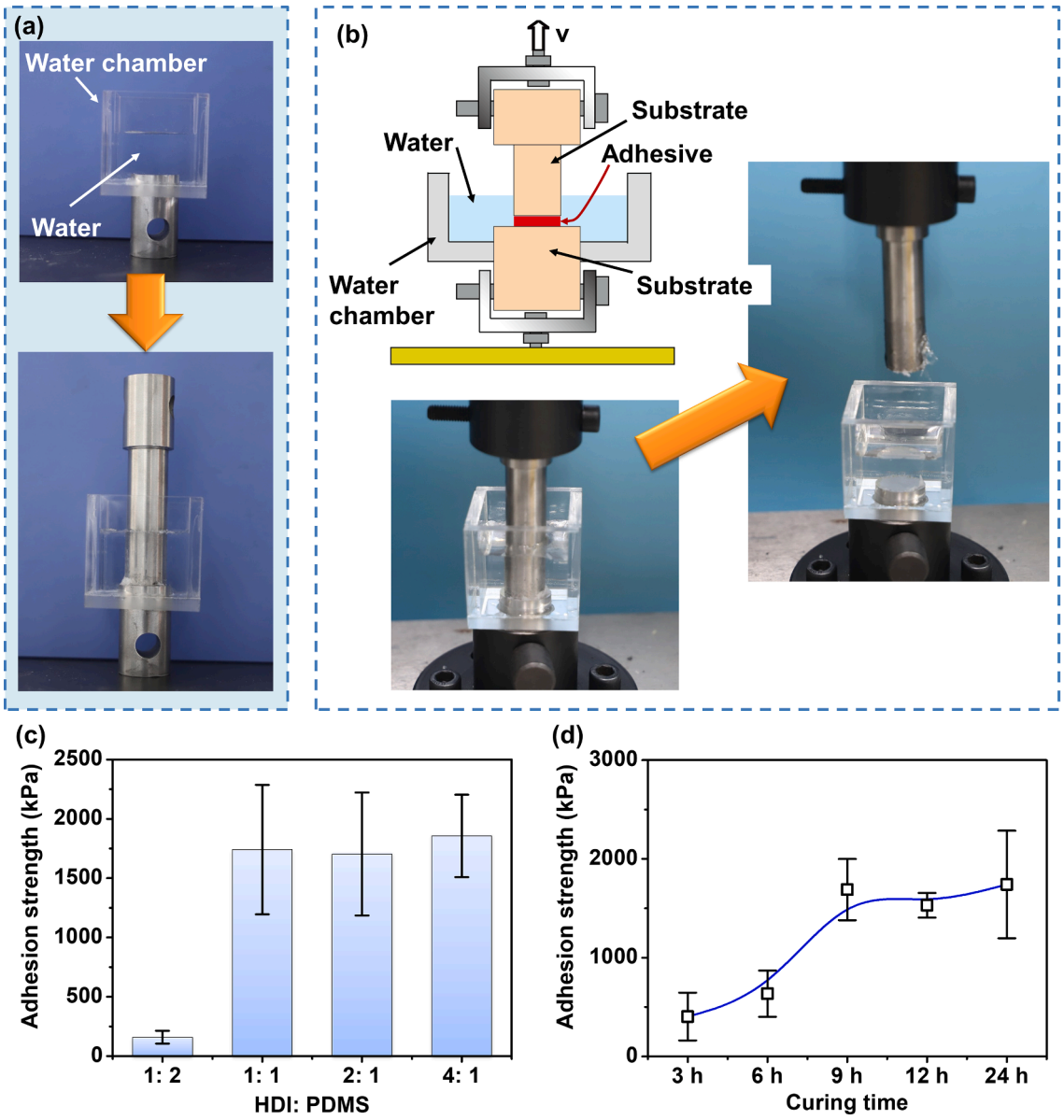

Fig. 4. The underwater tensile adhesion tests of the HDI-PDMS adhesives. (a) The adhesion tests were conducted by using a customized water chamber. (b) Schematic illustration and photos of the tensile adhesion tests. (c) The underwater tensile adhesion strengths of the adhesives at different HDI: PDMS ratios (1: 2, 1: 1, 2: 1 and 4: 1) on iron substrates with a curing time of 24 h. (d) The underwater tensile adhesion strength of the adhesive on iron with different curing times (3, 6, 9, 12 and 24 h, respectively).

assigned to the CH_2 groups [19–21]. For HDI, the absorption peaks at 2247 cm^{-1} and 1356 cm^{-1} are caused by N═C═O groups [22,23]. For PDMS and HDI-PDMS, the absorption peaks at 3327 cm^{-1} and 1630 cm^{-1} are resulted from the —NH— and —NH_2 groups [21,24,25]. The presence of absorption peaks at 1257 cm^{-1} and 767 ~ 786 cm^{-1} are due to Si—CH_3 groups [26–28]. Besides, the absorption peaks at 1008 ~ 1060 cm^{-1} is caused by Si—O—Si groups [26–28]. Compared with PDMS, the absorption peak of HDI-PDMS at 2043 cm^{-1} is assigned to the —N(C═O)N— groups in HDI-PDMS chains [22]. The FTIR results demonstrate that PDMS has reacted with HDI and new polymers have formed. In addition, XPS has been used to further examine the surface elemental composition of the HDI-PDMS adhesive, where Si 2p, Si 2s, N 1s, C 1s and O 1s peaks were observed (**Figure S3** in **Supporting Information**), which is related to the reaction occurred between PDMS and HDI.

3.2. *Underwater adhesion performance*

The fabricated HDI-PDMS adhesive can be painted on the substrate and instantly and firmly adhere two weights of 200 g and 500 g (see Fig. 2**a** and **Video S1**). Besides, the adhesive also showed excellent adhesiveness to various materials such as glass (Fig. 2**b**), iron (Fig. 2**c**), wood (Fig. 2**d**) and PTFE (Fig. 2**e**). In addition, the adhesive can also adhere pork bone underwater (**Figure S4**), showing potential in biomedical application. It should be noted that the adhesion strength of the adhesive is a function of curing time. Fig. 2**a** demonstrates that a 500 g weight can be instantly adhered and supported underwater using the adhesive. Generally, the adhesion strength would increase with the curing time. As shown in Fig. 3**a-b**, the adhesive is painted on a 2 kg weight underwater and a 200 g weight is immediately pressed against the surface. After curing for 8 min, the 2 kg weight can be easily lifted (see Fig. 3**c**) with an adhesion strength larger than 47 kPa. In addition, when the curing time is further extended to 24 h, a 10 kg weight can be

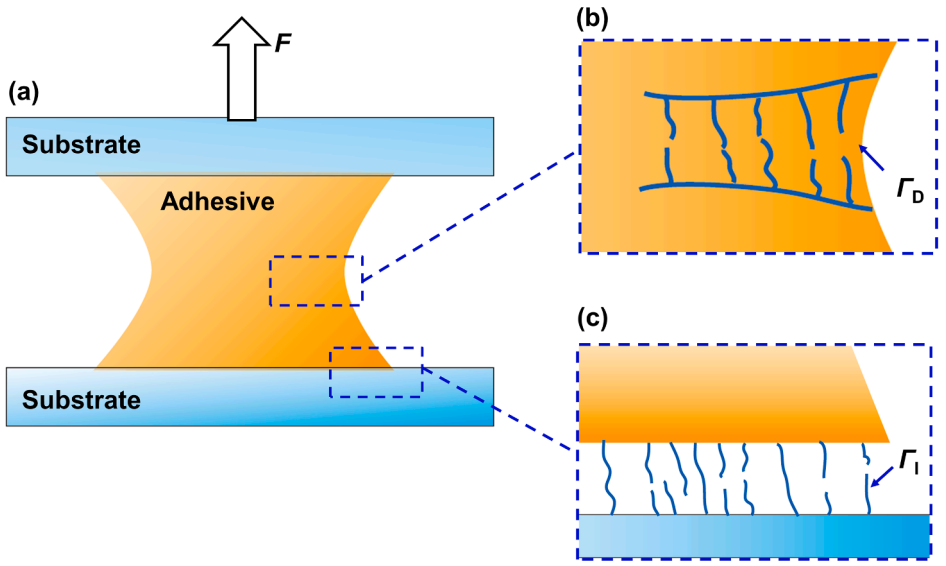

Fig. 5. (a) Schematic illustration of the deformation of the adhesive during tensile adhesion test. (b) The dissipated energy (Γ_D) for deforming and fracturing the adhesive. (c) The interfacial energy (Γ_I) required to overcome the interactions at the adhesive-substrate interface.

lifted by two adhered iron substrates (see Fig. 3**d**), exhibiting an adhesion strength larger than 554.6 kPa. Fig. 3**e** shows the adhesion failure at the interface after separation, where mixed interfacial failure (viz., cohesive failure and adhesive failure) is observed. As shown in Fig. 3**f**, the details of the mixed failure are imaged using an optical microscope, where the residual adhesive layer on the substrate can be observed. Because the fully cured adhesive is a type of hydrophobic polymers and not able to dissolve or degrade in water (**Figure S5a-b** in **Supporting Information**). The adhesive is stable underwater and suitable for long-term use, which can be demonstrated in **Figure S5c** in **Supporting Information**.

3.3. Underwater tensile adhesion tests

In order to quantitatively investigate the underwater adhesion strength of the HDI-PDMS adhesive, the tensile adhesion tests were conducted. It should be noted that all the processes were conducted underwater including painting, curing and testing. Fig. 4**a** shows the photos of the testing system, where a customized water chamber is used for the underwater adhesion test. Before testing, the samples were prepared by directly painting the adhesive on the substrate surface in water, pressing another substrate on the surface and curing for a certain time. Fig. 4**b** illustrates the scheme and photographs of the tensile adhesion tests underwater. To better understand the adhesion properties of the HDI-PDMS adhesive, the tests were firstly conducted based on the adhesive samples at different polymer molar ratios of HDI: PDMS = 1:2, 1:1, 2:1 and 4:1. As shown in Fig. 4**c**, the adhesion strengths of the adhesives with high HDI contents (1750 ± 500 kPa for HDI: PDMS = 1:1, 2:1 and 4:1) are much larger than that with a low HDI content (160 ± 50 kPa for HDI: PDMS = 1: 2). The adhesive at the HDI: PDMS ratio of 1: 1 is used as the model sample for further investigation in this work. As demonstrated in **Section 3.2**, the underwater adhesion strength of the adhesive is affected by curing time. In order to quantitatively understand the relation between adhesion strength and curing time, the underwater tensile adhesion tests with various curing times (3 h, 6 h, 9 h, 12 h and 24 h) were conducted. As shown in Fig. 4**d**, the adhesion strength firstly increased from ~ 400 kPa to ~ 1700 kPa when the curing time extended from 3 h to 9 h and then remained constant as the curing time further increased, indicating the adhesive was fully cured after 9 h. The polymer chains of the adhesive gradually grow during the curing process. Therefore, increasing the curing time will result in an increase in the molecular weight of polymer chains, which can be demonstrated by the increased viscosity of the adhesive (**Figure S6**). The increase in the molecular weight will also enhance the mechanical strength of the adhesive as well as the interactions at the interface, therefore enhancing the adhesion.

The adhesion strength of the adhesive at different curing times can be analyzed through the energy that required to break the adhesion (viz., the total adhesion energy). The total adhesion energy (Γ) can be expressed as follows [29,30],

$$\Gamma = \Gamma_I + \Gamma_D \tag{1}$$

where Γ_D is the dissipated energy for deforming and fracturing the adhesive (see Fig. 5**a-b**), and Γ_I is the interfacial energy required to overcome the interactions at the adhesive-substrate interface (see Fig. 5**c**). The interfacial energy is expressed as:[29]

$$\Gamma_I = U_I \cdot m(t) \tag{2}$$

where U_I is the energy required to fracture per unit bond at the interface, and $m(t)$ is the number of interaction bonds across a unit area. In addition, $m(t)$ is a function of curing time during the curing process of the adhesive at room temperature (25 °C). During the curing process, $m(t)$ would gradually increase owning to the decrease in monomer concentration and the increase in conversion of monomer [31,32], which can be expressed as:

$$m(t) = m - g_1 exp(-c_1 t^{2/3}) \tag{3}$$

where m is the number of interaction bonds across a unit area when the adhesive is fully cured, g_1 and c_1 are adjustable parameters. The detailed derivation process of **Equation (3)** is provided in **Supporting Information** (see **Equation S1-5**). In the tensile tests, the adhesive between the interfaces was deformed and fractured, and the dissipated energy (Γ_D) can be calculated as:[29]

$$\Gamma_D = \frac{U_{dc} N_{dc}(t) V}{A} \tag{4}$$

where U_{dc} is the dissipated energy required to deform and fracture a polymer chain of the adhesive. $N_{dc}(t)$ is the number of polymer chains that required to fracture per unit volume, V is the volume of adhesive, and A is the contact area of the tensile tests. It should be noted that $N_{dc}(t)$ is a function of curing time during the curing process of the adhesive at room temperature (25 °C), which can be expressed as:[31,32]

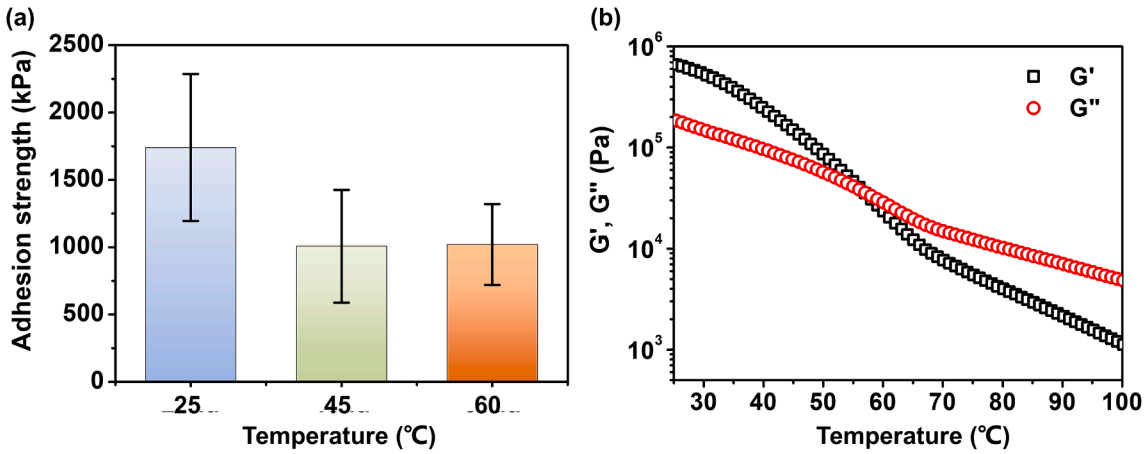

Fig. 6. (a) The underwater tensile adhesion strength of the adhesive on iron at different temperatures (25 °C, 45 °C and 60 °C). The tests were carried out in water with a curing time of 24 h. (b) The storage modulus (G′) and loss modulus (G″) of the cured adhesive decreased as the temperature increased.

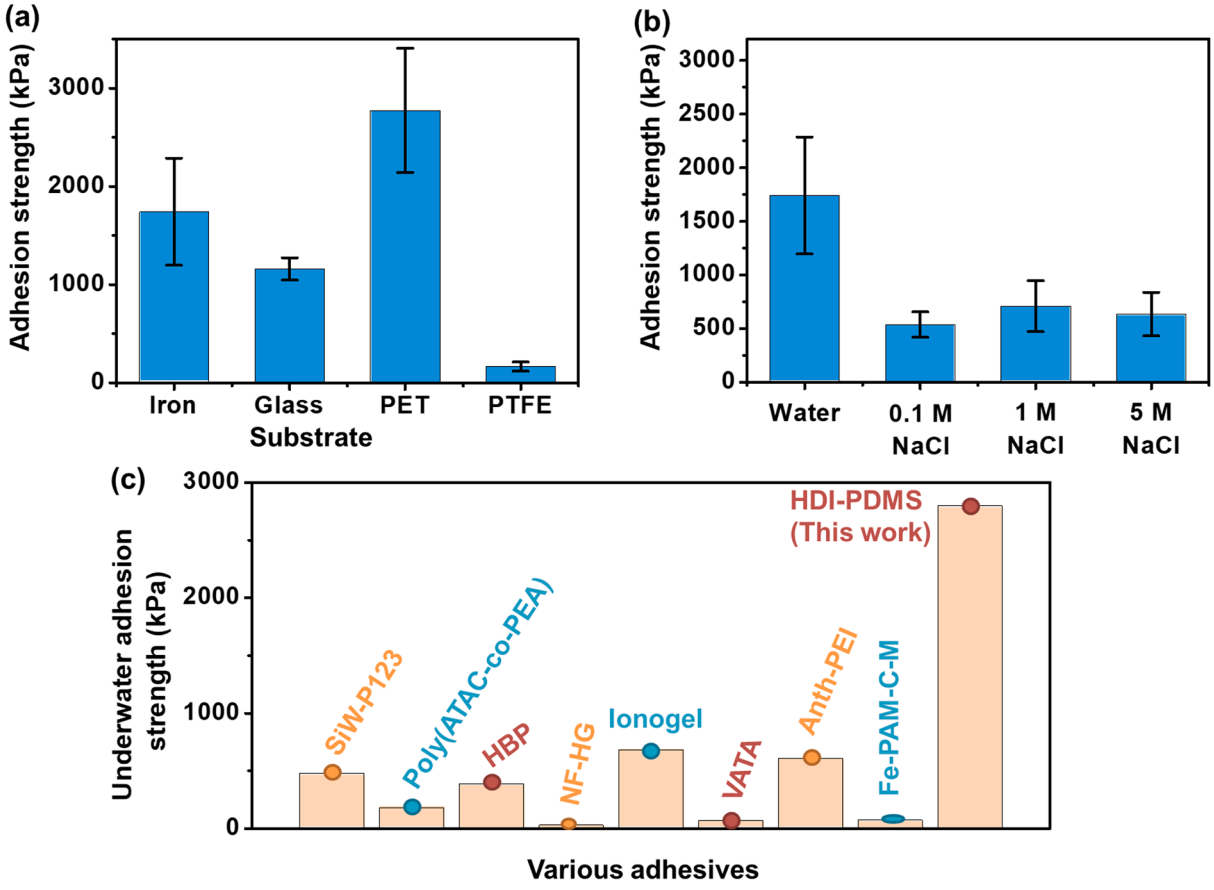

Fig. 7. (a) The underwater tensile adhesion strength of the adhesive on different substrates including iron, glass, PET and PTFE with a curing time of 24 h. The tests were carried out in water at room temperature (25 °C). (b) The underwater tensile adhesion strength of the adhesive on iron in different aqueous solutions (water, 0.1 M NaCl, 1 M NaCl, 5 M NaCl). (c) Comparison of the highest underwater adhesion strength of various adhesives reported in recent literatures and the HDI-PDMS adhesive in this work. The adhesives reported in the literatures including SiW-P123 [13], poly(ATAC-co-PEA) [17], HBP [18], NF-HG [46], ionogel [47], VATA [48], anth-PEI [49] and Fe-PAM-C-M [50] adhesives.

$$N_{dc}(t) = N_{dc} - g_2 exp(-c_2 t^{2/3}) \quad (5)$$

where N_{dc} is the number of polymer chains that required to fracture per unit volume when the adhesive is fully cured, g_2 and c_2 are adjustable parameters. The detailed derivations about **Equation (5)** are provided in **Supporting Information** (see **Equation S1-5**). The total adhesion energy (Γ) can be expressed by combining **Equation (1)–(5)** as:

$$\Gamma = \left(U_1 m + \frac{U_{dc} N_{dc} V}{A}\right) - \left(U_1 g_1 + \frac{U_{dc} V g_2}{A}\right)\left(exp(-c_1 t^{2/3}) + exp(-c_2 t^{2/3})\right) \quad (6)$$

As expressed by **Equation (6)**, extending the curing time (t) of the adhesive would increase the adhesion energy (Γ), therefore enhancing the adhesion strength.

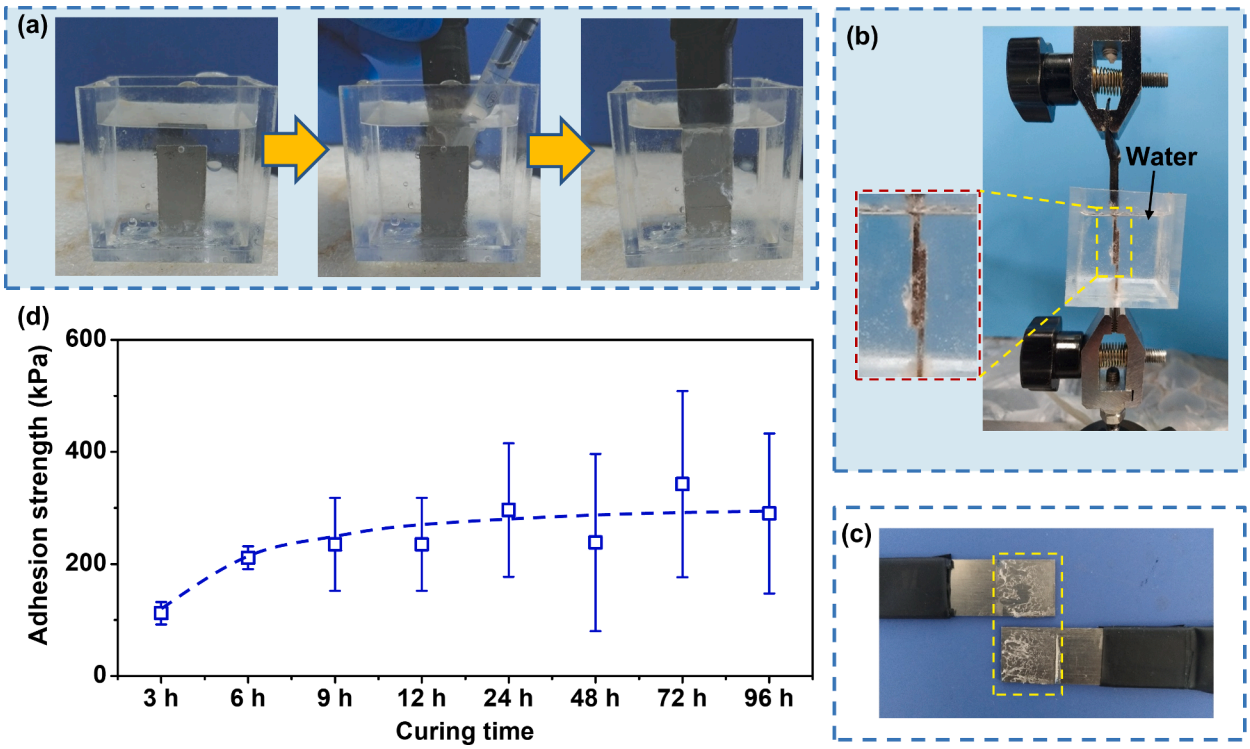

Fig. 8. The underwater lap-shear adhesion tests of the HDI-PDMS polymeric adhesive. (a) The adhesive was injected and painted on the surface of the substrates, followed by curing. The process was conducted underwater in a water chamber. (b) Photos of the underwater lap-shear adhesion test and (c) adhesion failure. (d) The underwater lap-shear adhesion strength of the adhesive on iron as a function of curing time. All the tests were carried in water at room temperature (25 °C).

In addition, the adhesion strength of the adhesive is also a function of the temperature. Fig. 6**a** shows the underwater adhesion strengths of the adhesive on iron at 25 °C, 45 °C and 60 °C, respectively. It can be observed that the adhesion strength at high temperatures (e.g. 45 °C, 60 °C) is much lower than that at room temperature (25 °C), which is caused by the decrease in the modulus of the cured adhesive at high temperature. As shown in Fig. 6**b**, both storage modulus (G′) and loss modulus (G″) of the cured adhesive decreased as the temperature increased, therefore leading to a decrease in adhesive strength. In addition, increasing the temperature can also decrease the interaction at the interface [33–35], which leads to the decrease in interfacial adhesion. For underwater adhesion, the practical temperature is in the range of 0 ~ 100 °C. TG results show that the adhesive will not degrade and can maintain stable when the temperature is lower than 200 °C (**Figure S7** in Supporting Information). Therefore, the underwater adhesive is suitable for practical underwater applications.

Fig. 7**a** shows underwater tensile adhesion strength of the adhesive on the typical substrates including iron, glass, PET and PTFE. It can be observed that the adhesion strength of the adhesive on PET is the highest (2800 ± 600 kPa) among the tested substrates, which is mainly due to the combination of hydrogen bonds (**Figure S8a**) [13,33,36,37], and topological adhesion (**Figure S8b**) [38,39]. Besides, the covalent bonds formed by the O═C═N— of the adhesive and —OH on the substrate also works at the interface (see **Figure S8c**). For the iron substrates, metal complexation and chemical crosslinks (e.g. —NH—COO—Fe, —N═Fe and —NH—Fe) mainly works at the interface (see **Figure S9**), and the measured adhesion strength is 1750 ± 500 kPa. In addition, the underwater adhesion strength of the adhesive on glass is 1160 ± 115 kPa, and chemical crosslinks (e.g. –NH-COO-Si) and hydrogen bonds mainly contribute to the underwater adhesion (see **Figure S10**) [40–42]. The underwater adhesion strength of the adhesive on PTFE (163 ± 47 kPa) is much lower than that on other substrates, which is caused by the low surface energy of PTFE substrate (~19 mJ/m^2 [43]). Details about the adhesion mechanism of the adhesive on those substrates are discussed in Section 3.5. In addition, the effect of salts on the underwater adhesion strength is investigated by using NaCl aqueous solutions. As shown in Fig. 7**b**, the underwater adhesion strength dramatically decreases from 1750 ± 500 kPa to 700 ± 200 kPa when NaCl solution is used in the tests. The addition of NaCl can form layers of hydrated ions at the interfaces and impair the interactions by screening the electrostatic charges on the polymer chains and the substrate surface [44,45]. In addition, the adhesion strength is nearly unchanged when the NaCl concentration further increased from 0.1 M to 5 M. The result indicates that ions salt concentration in 0.1 M NaCl solution is enough to screen the electrostatic charges at the interface. Recent literatures have reported quite a few underwater adhesives, and the highest underwater adhesion strength are shown and compared with the results described in this work [13,17,18,46–50]. As shown in Fig. 7**c** and **Table S2** (Supporting Information), the underwater adhesion strengths of the recently-reported adhesives (named as SiW-P123 [13], poly(ATAC-co-PEA) [17], HBP [18], NF-HG [46], ionogel [47], VATA [48], anth-PEI [49] and Fe-PAM-C-M [50]) are <1 MPa. Compared with these underwater adhesives, the HDI-PDMS adhesive developed in this work exhibits superior underwater adhesion with a highest adhesion strength of 2.8 MPa. The HDI-PDMS underwater adhesive shows great potential in biomedical and engineering applications.

3.4. Underwater lap-shear adhesion tests

Underwater lap-shear adhesion tests of the adhesive were also conducted to better understand the adhesion property of the adhesive. As shown in Fig. 8**a**, the testing substrates are adhered by the HDI-PDMS adhesive in water, followed by curing for certain amount of time. After that, the samples are used to conduct the lap-shear tests (see Fig. 8**b**). The results show that the adhesion failure occurred within the adhesive layer (viz., cohesive failure occurred, see Fig. 8**c**). Similar to the tensile testing results, the lap-shear adhesion strength is also a function of curing time. As shown in Fig. 8**d**, the lap-shear adhesion

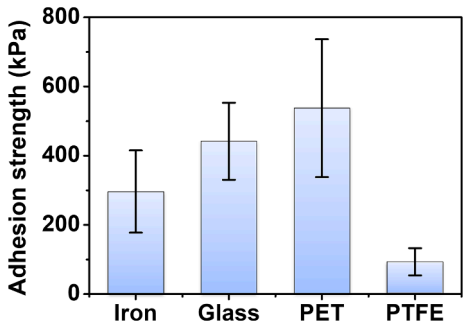

Fig. 9. The underwater lap-shear adhesion strength of the adhesive on different substrates including iron, glass, PET and PTFE after curing for 24 h. The tests were carried in water at room temperature (25 °C).

strength of the adhesive on iron gradually increases from 112 ± 20 kPa to 300 ± 120 kPa when the curing time increases from 3 h to 24 h, and then the adhesion strength almost remains as a constant. As discussed in Section 3.3, extending the curing time can increase the number of interaction bonds, therefore enhancing the interactions at the interface. In addition, the mechanical strength of the adhesive increases with curing time, which can also enhance the lap-shear adhesion strength. When the curing time reached 24 h, the adhesion strength would no further increase since the adhesive is fully cured. Fig. 9 shows the lap-shear adhesion strength of the adhesive on different substrates. The result shows that the lap-shear adhesion of the adhesive on PET (573 ± 199 kPa) is higher than that on glass (441 ± 111 kPa) and iron (296 ± 119 kPa), which is consistent with the tensile adhesion tests in Section 3.3. For the PTFE substrate, the lap-shear adhesion strength is quite low (93 ± 40 kPa), which is likely due to the low surface energy of PTFE (~19 mJ/m^2 [43]). The underwater adhesion of the adhesive is mainly attributed to the combination of chemical crosslinks, hydrogen bonds and other physical interactions, which will be discussed in detail in Section 3.5.

3.5. Underwater adhesion mechanism

Fig. 10 shows the schematic illustration of the proposed underwater adhesion mechanism for HDI-PDMS adhesive. In aqueous solutions, the substrate is generally covered with layers of absorbed water molecules, and the —OH groups on the surface can react with the unreacted isocyanate groups in HDI-PDMS. As shown in Fig. 10**a**, when the adhesive is painted on the substrate, reactions between the O═C═N— groups of the polymer chains and —OH groups on the substrate would occur. Chemical crosslinks including R—NH— and R—NH—COO— are formed at the interface. For the R—NH— crosslinks, the reaction occurs in two steps as shown below [40,41,51],

$$R—N═C═O + H_2O \rightarrow R—NH_2 + CO_2 \quad (7)$$

$$R—NH_2 + —OH \rightarrow R—NH— + H_2O \quad (8)$$

Firstly, the O═C═N— groups react with the absorbed water on the substrate and —NH_2 groups are generated (**Equation 7**) [51]. After that, —NH_2 groups react with —OH on the substrate to form R—NH— crosslinks (**Equation 8**) [51]. In addition, R—NH—COO— crosslinks can be formed through the electrophilic addition reaction between O═C═N— groups and —OH groups as follows [40,51],

$$R—N═C═O + —OH \rightarrow R—NH—COO— \quad (9)$$

In addition, other physical interactions also contribute to the adhesion. Fig. 10**b** shows the possible interactions at the interface including chemical crosslinks, hydrogen bonds and other physical interactions. The O═C═N— groups in the adhesive polymer can form chemical crosslinks with the substrates (e.g. —NH—COO—). For some Si-containing substrates (e.g. glass, quartz and silicon), —NH—COO—Si

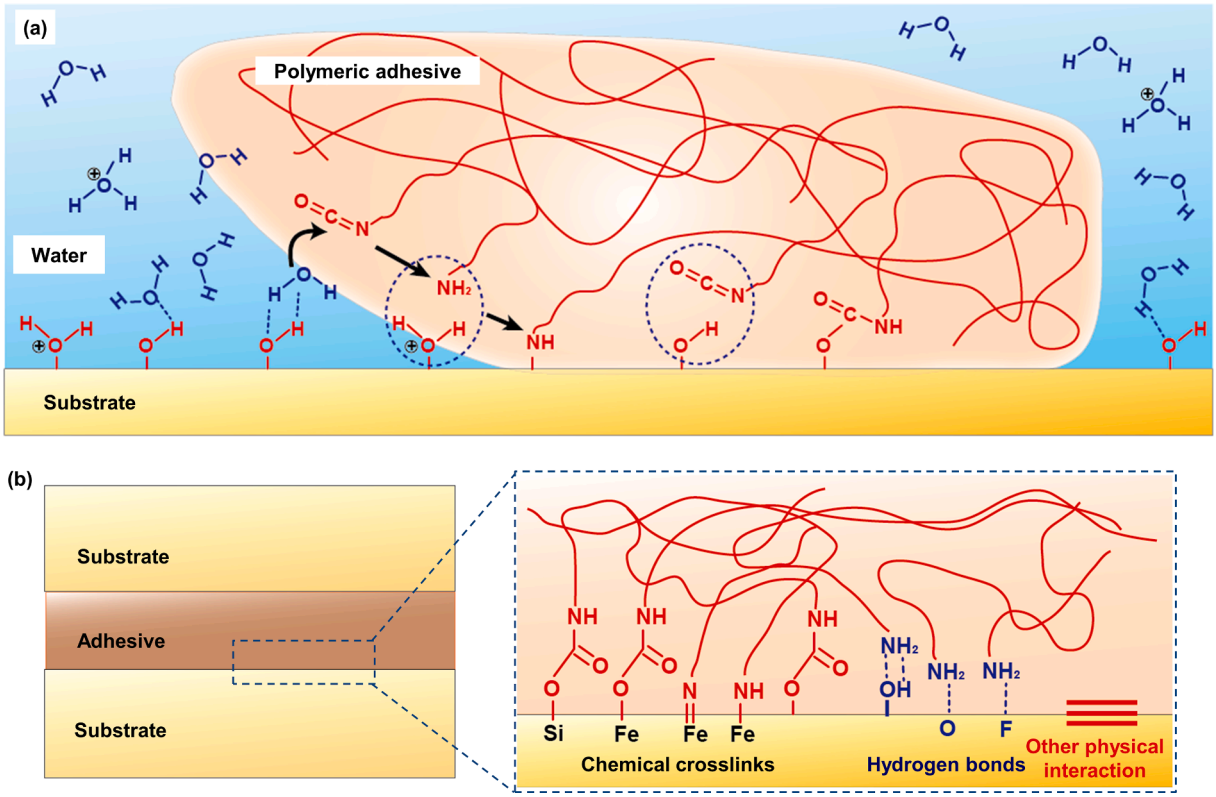

Fig. 10. Schematic illustration of the proposed underwater adhesion mechanism. (a) The formation of the chemical crosslinks at the interface. (b) Possible interactions at the interface including chemical crosslinks, hydrogen bonds and other physical interactions.

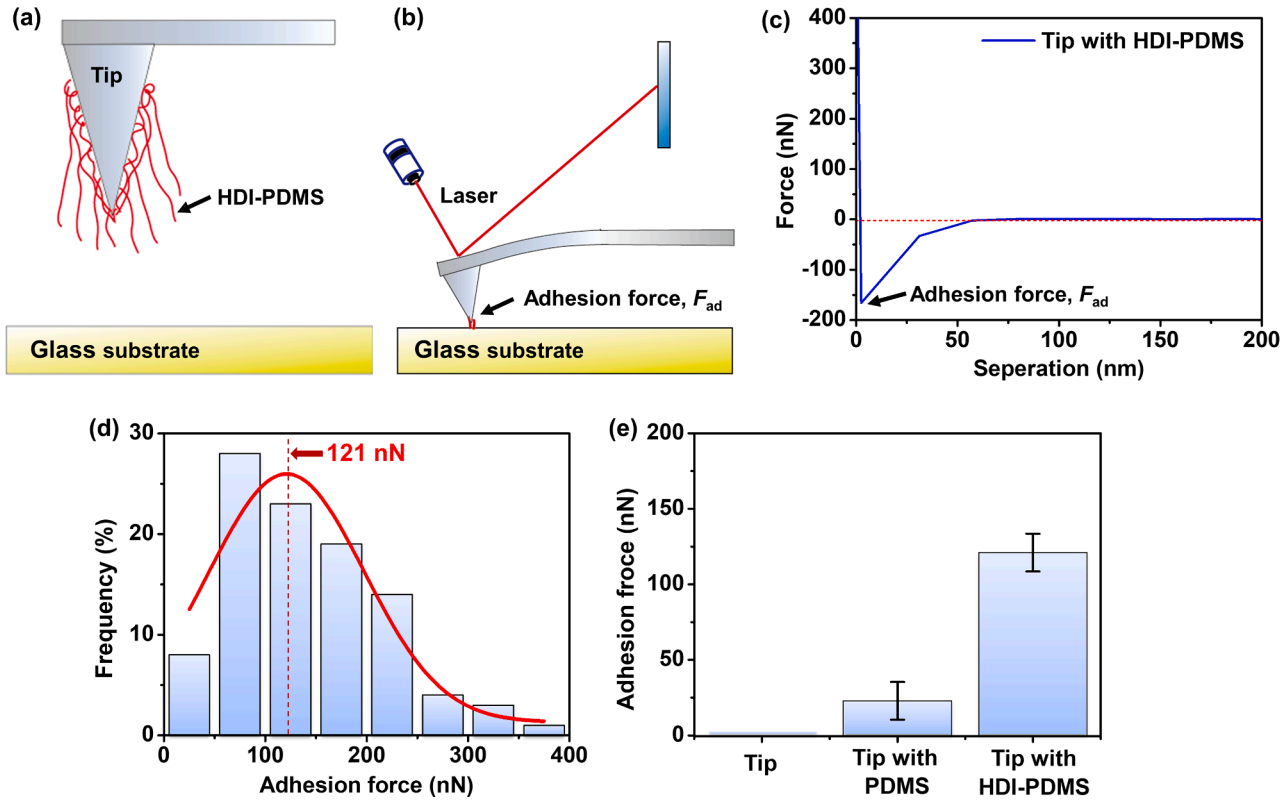

Fig. 11. (a) Schematic illustration of an AFM tip coated with HDI-PDMS adhesive, and (b) adhesion force measurements of HDI-PDMS adhesive on the glass surface. (c) Typical force-separation curve for the tip with HDI-PDMS on the glass substrate. (d) The distribution of adhesion forces and fitted Gaussian distribution for the tip with HDI-PDMS on the glass substrate. (e) The adhesion force for the tip, tip with PDMS and tip with HDI-PDMS on glass substrates.

can be formed at the interface [40]. For the iron substrate, some chemical crosslinks including —NH—COO—Fe, —N═Fe and —NH—Fe also contribute to the underwater addition [40,52]. Besides, —NH—, —NH_2 and C═O function groups in the adhesive polymer can form hydrogen bonds with the substrate at the interface [36,37,42,53]. Additionally, other physical interactions including metal complexation and van der Waals interaction could also contribute to the underwater adhesion. For PTFE or some other fluorine-containing substrates, the dipole–dipole interactions between fluorine atoms in substrates and hydrogen atoms in the adhesive polymer can enhance the van der Waals interactions. Therefore, the measured underwater adhesion is due to the combination of chemical crosslinks, hydrogen bonds and other physical interactions (see Fig. 10**b**).

To further characterize the adhesion behavior of the HDI-PDMS adhesive from the microscale, a silicon AFM tip coated with HDI-PDMS is used to measure the interaction with a glass surface (Fig. 11**a-b**). Fig. 11**c** shows a typical separation curve for HDI-PDMS interacting with a glass surface. An adhesion force of over 150 nN is observed. And the measured adhesion forces between HDI-PDMS and glass surface are plotted in the histogram and fitted with Gaussian distribution (see Fig. 11**d**). Fig. 11**e** shows the measured adhesion force between the glass substrate with the silicon tip, PDMS and HDI-PDMS. The measured adhesion force on glass substrate during separation is as follows: silicon < PDMS < HDI-PDMS. For the neat silicon tip, the adhesion force at the interface is too small to be measured. The adhesion force between PDMS and the glass surface is 22.9 ± 12.5 nN due to the hydrogen bonds. For HDI-PDMS, the adhesion force is 121 ± 12.5 nN, which is mainly caused by chemical crosslinks and hydrogen bonds. The AFM force measurement result is consistent with the tensile adhesion tests, that the HDI-PDMS exhibits strong adhesion with the substrates.

4. Conclusion

In summary, we have developed a strong underwater adhesive by modifying bis(3-aminopropyl) terminated PDMS with HDI. The obtained HDI-PDMS adhesive can be totally cured in aqueous solution and shows excellent underwater adhesion on various substrates (e.g. glass, iron, PET and PTFE) due to the combination of chemical crosslinks, hydrogen bonds and other physical interactions. Results show that the highest underwater adhesion strength of the adhesive on PET substrates is 2.8 MPa, which is comparable with commercially available adhesives that cured in air. In addition, the adhesion strength increases with curing time, which is caused by the enhanced interactions at the interface and the increased mechanical strength of the adhesive. Besides, the ions in saline solution would impair the interactions at the interface by screening of the electrostatic charges on the polymer chains and the substrate surface. Furthermore, the AFM force measurements also showed a strong adhesion between the HDI-PDMS adhesive and the glass surface from the microscale, which is consistent with the tensile adhesion tests. Our work provides a facile method of fabricating underwater adhesive, improving the fundamental understanding of polymeric underwater adhesives. For future study, single molecular forces combining with theoretical simulations would provide useful guidance on further revealing the underwater adhesion mechanism from the molecular level.

Declaration of Competing Interest

The authors declare that they have no known competing financial interests or personal relationships that could have appeared to influence the work reported in this paper.

Acknowledgements

This work was supported by the National Natural Science Foundation of China (No. 51905305), the Natural Science Foundation of Shandong Province (No. ZR2020YQ38, ZR2019ZD36), the General Program of National Natural Science Foundation of China (81772093), the Open Fund of Key Laboratory of Icing and Anti/De-icing(Grant No. 2001IADL20200401), and Key Laboratory of High-efficiency and Clean Mechanical Manufacture at Shandong University, Ministry of Education China.

Appendix A. Supplementary data

Supplementary data to this article can be found online at https://doi.org/10.1016/j.cej.2021.133460.

References

[1] P. Rao, T.L. Sun, L. Chen, R. Takahashi, G. Shinohara, H. Guo, D.R. King, T. Kurokawa, J.P. Gong, Tough hydrogels with fast, strong, and reversible underwater adhesion based on a multiscale design, Adv. Mater. 30 (2018) 1801884.
[2] Y. Zhao, Y. Wu, L. Wang, M. Zhang, X. Chen, M. Liu, J. Fan, J. Liu, F. Zhou, Z. Wang, Bio-inspired reversible underwater adhesive, Nat. Commun. 8 (2017) 1–8.
[3] W. Wei, L. Petrone, Y. Tan, H. Cai, J.N. Israelachvili, A. Miserez, J.H. Waite, An underwater surface-drying peptide inspired by a mussel adhesive protein, Adv. Funct. Mater. 26 (20) (2016) 3496–3507.
[4] R.J. Stewart, T.C. Ransom, V. Hlady, Natural underwater adhesives, J. Polym. Sci., Part B: Polym. Phys. 49 (11) (2011) 757–771.
[5] A.H. Hofman, I.A. van Hees, J. Yang, M. Kamperman, Bioinspired underwater adhesives by using the supramolecular toolbox, Adv. Mater. 30 (2018) 1704640.
[6] A. Cholewinski, F. Yang, B. Zhao, Algae–mussel-inspired hydrogel composite glue for underwater bonding, Mater. Horiz. 6 (2) (2019) 285–293.
[7] C. Fan, J. Fu, W. Zhu, D.A. Wang, A mussel-inspired double-crosslinked tissue adhesive intended for internal medical use, Acta Biomater. 33 (2016) 51–63.
[8] P. Kord Forooshani, B.P. Lee, Recent approaches in designing bioadhesive materials inspired by mussel adhesive protein, J. Polym. Sci., Part A: Polym. Chem. 55 (1) (2017) 9–33.
[9] H.G. Silverman, F.F. Roberto, Understanding marine mussel adhesion, Mar. Biotechnol. 9 (6) (2007) 661–681.
[10] X. Cui, J. Liu, L. Xie, J. Huang, Q. Liu, J.N. Israelachvili, H. Zeng, Modulation of hydrophobic interaction by mediating surface nanoscale structure and chemistry, not monotonically by hydrophobicity, Angew. Chem. 130 (37) (2018) 12079–12084.
[11] B. Yan, J. Huang, L. Han, L.u. Gong, L. Li, J.N. Israelachvili, H. Zeng, Duplicating dynamic strain-stiffening behavior and nanomechanics of biological tissues in a synthetic self-healing flexible network hydrogel, ACS Nano 11 (11) (2017) 11074–11081.
[12] S. Kim, J. Huang, Y. Lee, S. Dutta, H.Y. Yoo, Y.M. Jung, Y.S. Jho, H. Zeng, D. S. Hwang, Complexation and coacervation of like-charged polyelectrolytes inspired by mussels, Proc. Natl. Acad. Sci. U.S.A. 113 (7) (2016) E847–E853.
[13] Q. Peng, J. Chen, T. Wang, L. Gong, X. Peng, M. Wu, Y. Ma, F. Wu, D. Yang, H. Zhang, H. Zeng, Coacervation-driven instant paintable underwater adhesives with tunable optical and electrochromic properties, J. Mater. Chem. A 9 (22) (2021) 12988–13000.
[14] H. Zhao, Y. Wei, C. Wang, R. Qiao, W. Yang, P.B. Messersmith, G. Liu, Mussel-inspired conductive polymer binder for Si-alloy anode in lithium-ion batteries, ACS Appl. Mater. Inter. 10 (6) (2018) 5440–5446.
[15] L. Han, K. Liu, M. Wang, K. Wang, L. Fang, H. Chen, J. Zhou, X. Lu, Mussel-inspired adhesive and conductive hydrogel with long-lasting moisture and extreme temperature tolerance, Adv. Funct. Mater. 28 (2018) 1704195.
[16] M. Dompé, F.J. Cedano-Serrano, O. Heckert, N. van den Heuvel, J. van der Gucht, Y. Tran, D. Hourdet, C. Creton, M. Kamperman, Thermoresponsive complex coacervate-based underwater adhesive, Adv. Mater. 31 (2019) 1808179.
[17] H. Fan, J. Wang, J.P. Gong, Barnacle cement proteins-inspired tough hydrogels with robust, long-lasting, and repeatable underwater adhesion, Adv. Funct. Mater. 31 (2021) 2009334.
[18] C. Cui, C. Fan, Y. Wu, M. Xiao, T. Wu, D. Zhang, X. Chen, B. Liu, Z. Xu, B. Qu, Water-triggered hyperbranched polymer universal adhesives: from strong underwater adhesion to rapid sealing hemostasis, Adv. Mater. 31 (2019) 1905761.
[19] Y. Yan, S. Xu, H. Liu, X. Cui, J. Shao, P. Yao, J. Huang, X. Qiu, C. Huang, A multi-functional reversible hydrogel adhesive, Colloids Surf., A 593 (2020), 124622.
[20] J. Huang, X. Qiu, B. Yan, L. Xie, J. Yang, H. Xu, Y. Deng, L. Chen, X. Wang, H. Zeng, Robust polymer nanofilms with bioengineering and environmental applications via facile and highly efficient covalent layer-by-layer assembly, J. Mater. Chem. B 6 (22) (2018) 3742–3750.
[21] D.R. Biswal, R.P. Singh, Characterisation of carboxymethyl cellulose and polyacrylamide graft copolymer, Carbohydr. Polym. 57 (4) (2004) 379–387.
[22] J. Ederer, P. Janoš, P. Ecorchard, J. Tolasz, V. Štengl, H. Beneš, M. Perchacz, O. Pop-Georgievski, Determination of amino groups on functionalized graphene oxide for polyurethane nanomaterials: XPS quantitation vs. functional speciation, RSC Adv. 7 (2017) 12464–12473.
[23] D. Sun, J. An, G. Wu, J. Yang, Double-layered reactive microcapsules with excellent thermal and non-polar solvent resistance for self-healing coatings, J. Mater. Chem. A 3 (8) (2015) 4435–4444.
[24] Z. Yang, H. Yang, Z. Jiang, T. Cai, H. Li, H. Li, A. Li, R. Cheng, Flocculation of both anionic and cationic dyes in aqueous solutions by the amphoteric grafting flocculant carboxymethyl chitosan-graft-polyacrylamide, J. Hazard. Mater. 254-255 (2013) 36–45.
[25] S.H. Shaikh, S.A. Kumar, Polyhydroxamic acid functionalized sorbent for effective removal of chromium from ground water and chromic acid cleaning bath, Chem. Eng. J. 326 (2017) 318–328.
[26] L.M. Johnson, L. Gao, C.W. Shields IV, M. Smith, K. Efimenko, K. Cushing, J. Genzer, G.P. López, Elastomeric microparticles for acoustic mediated bioseparations, J. Nanobiotechnol. 11 (2013) 1–8.
[27] J.J.H. Lancastre, N. Fernandes, F.M.A. Margaça, I.M. Miranda Salvado, L. M. Ferreira, A.N. Falcão, M.H. Casimiro, Study of PDMS conformation in PDMS-based hybrid materials prepared by gamma irradiation, Radiat. Phys. Chem. 81 (9) (2012) 1336–1340.
[28] N. Atthi, W. Sripumkhai, P. Pattamang, O. Thongsook, R. Meananeatra, P. Saengdee, A. Srihapat, J. Supadech, T. Janseng, A. Maneesong, Superhydrophobic and superoleophobic properties enhancement on PDMS micro-structure using simple flame treatment method, Microelectron. Eng. 230 (2020), 111362.
[29] X. Zhao, Multi-scale multi-mechanism design of tough hydrogels: building dissipation into stretchy networks, Soft Matter 10 (2014) 672–687.
[30] H. Yuk, T. Zhang, S. Lin, G.A. Parada, X. Zhao, Tough bonding of hydrogels to diverse non-porous surfaces, Nat. Mater. 15 (2016) 190–196.
[31] D. Gigmes, D. Bertin, C. Lefay, Y. Guillaneuf, Kinetic modeling of nitroxide-mediated polymerization: conditions for living and controlled polymerization, Macromol. Theory Simul. 18 (7-8) (2009) 402–419.
[32] H. Fischer, The persistent radical effect in controlled radical polymerizations, J. Polym. Sci., Part A: Polym. Chem. 37 (13) (1999) 1885–1901.
[33] Y. Yan, J. Huang, X. Qiu, X. Cui, S. Xu, X. Wu, P. Yao, C. Huang, An ultra-stretchable glycerol-ionic hybrid hydrogel with reversible gelid adhesion, J. Colloid Interface Sci. 582 (2021) 187–200.
[34] C. Tang, X. Li, Z. Li, W. Tian, Q. Zhou, Molecular simulation on the thermal stability of meta-aramid insulation paper fiber at transformer operating temperature, Polymers 10 (2018) 1348.
[35] M. Huš, T. Urbic, Strength of hydrogen bonds of water depends on local environment, J. Chem. Phys. 136 (2012), 144305.
[36] X. Liu, Q. Zhang, Z. Gao, R. Hou, G. Gao, Bioinspired adhesive hydrogel driven by adenine and thymine, ACS Appl. Mater. Inter. 9 (20) (2017) 17645–17652.
[37] C. Heinzmann, C. Weder, L.M. de Espinosa, Supramolecular polymer adhesives: advanced materials inspired by nature, Chem. Soc. Rev. 45 (2016) 342–358.
[38] J. Steck, J. Yang, Z. Suo, Covalent topological adhesion, ACS Macro Lett. 8 (6) (2019) 754–758.
[39] J. Steck, J. Kim, J. Yang, S. Hassan, Z. Suo, Topological adhesion. I. Rapid and strong topohesives, Extreme Mech. Lett. 39 (2020), 100803.
[40] G. Zhang, A. Dass, A.M. Rawashdeh, J. Thomas, J.A. Counsil, C. Sotiriou-Leventis, E.F. Fabrizio, F. Ilhan, Pl. Vassilaras, D.A. Scheiman, L. McCorkle, A. Palczer, J. C. Johnston, M.A. Meador, N. Leventis, Isocyanate-crosslinked silica aerogel monoliths: preparation and characterization, J. Non-Cryst. Solids 350 (2004) 152–164.
[41] C. Nies, C. Wehlack, H. Ehbing, D.J. Dijkstra, W. Possart, Adhesive interactions of polyurethane monomers with native metal surfaces, J. Adhesion 88 (8) (2012) 665–683.
[42] Y. Yan, J. Cui, X. Qiu, H. Liu, X. Liu, P. Yao, J. Huang, X. Cui, X. Liang, C. Huang, Towards large-scale fabrication of self-healable functional hydrogel coatings for anti-fog/frost surfaces and flexible sensors, Adv. Mater. Technol. 6 (7) (2021) 2001267.
[43] H. Zeng, Polymer Adhesion, Friction, and Lubrication, John Wiley & Sons, 2013.
[44] L. Han, B. Yan, L. Zhang, M. Wu, J. Wang, J. Huang, Y. Deng, H. Zeng, Tuning protein adsorption on charged polyelectrolyte brushes via salinity adjustment, Colloids Surf. A 539 (2018) 37–45.
[45] L. Alfhaid, N.H. Williams, M. Geoghegan, Adhesion between oppositely charged polyelectrolytes in salt solution, J. Appl. Polym. Sci. 137 (2020) 49130.
[46] Y. Chen, H. Qin, A. Mensaha, Q. Wang, F. Huang, Q. Wei, Biomimetic nanocomposite hydrogel networks for robust wet adhesion to tissues, Compos. B. Eng. 222 (2021) 109071.
[47] Z. Yu, P. Wu, Underwater Communication and Optical Camouflage Ionogels, Adv. Mater. 33 (24) (2021) 2008479.
[48] D. Lee, H. Hwang, J.-S. Kim, J. Park, D. Youn, D. Kim, J. Hahn, M. Seo, H. Lee, VATA: a poly (vinyl alcohol)-and tannic acid-based nontoxic underwater adhesive, ACS Appl. Mater. Inter. 12 (2020) 20933–20941.
[49] Z. Wang, L. Guo, H. Xiao, H. Cong, S. Wang, A reversible underwater glue based on photo-and thermo-responsive dynamic covalent bonds, Mater. Horiz. 7 (1) (2020) 282–288.
[50] L. Han, M. Wang, L.O. Prieto-López, X. Deng, J. Cui, Self-hydrophobization in a dynamic hydrogel for creating nonspecific repeatable underwater adhesion, Adv. Funct. Mater. 30 (2020) 1907064.
[51] J. Bañuls-Ciscar, G.F. Trindade, M.-L. Abel, C. Phanopoulos, G. Pans, D. Pratelli, K. Marcoen, T. Hauffman, J.F. Watts, A study of the interfacial chemistry between

polymeric methylene diphenyl di-isocyanate and a Fe–Cr alloy, Surf. Interface Anal. 53 (3) (2021) 340–349.
[52] S. Tardio, M.-L. Abel, R.H. Carr, J.F. Watts, The interfacial interaction between isocyanate and stainless steel, Int. J. Adhes. Adhes. 88 (2019) 1–10.
[53] J. Chen, J. Liu, T. Thundat, H. Zeng, Polypyrrole-doped conductive supramolecular elastomer with stretchability, rapid self-healing, and adhesive property for flexible electronic sensors, ACS Appl. Mater. Inter. 11 (20) (2019) 18720–18729.